

Core-hole screening response in two-dimensional cuprates: A high-resolution x-ray photoemission study

A. Koitzsch and J. Fink

Institute for Solid State Research, IFW Dresden, P.O. Box 270016, D-01171 Dresden, Germany

M. S. Golden

Van der Waals-Zeeman Institute, University of Amsterdam, Valckenierstraat 65, NL-1018 XE Amsterdam, The Netherlands

K. Karlsson

Institutionen för Naturvetenskap, Högskolan Skövde, S-541 28 Skövde, Sweden

O. Jepsen and O. Gunnarsson

Max-Planck-Institut für Festkörperforschung, Heisenbergstrasse 1, D-70569 Stuttgart, Germany

L. L. Miller

Ames Laboratory, Iowa State University, Ames, Iowa 50011

H. Eisaki

Department of Applied Physics, Stanford University, Stanford, California 94305-4090

S. Uchida

Department of Superconductivity, The University of Tokyo, Bunkyo-ku, Tokyo 113, Japan

G. Yang and S. Abell

School of Metallurgy and Materials, The University of Birmingham, Birmingham, B15 2TT, United Kingdom

(Received 29 October 2001; published 25 July 2002)

We have studied the core level photoemission spectra of the two-dimensional cuprates $\text{Sr}_2\text{CuO}_2\text{Cl}_2$, $\text{Sr}_2\text{CuO}_2\text{Br}_2$, $\text{Ca}_2\text{CuO}_2\text{Cl}_2$, $\text{Bi}_2\text{Sr}_2\text{CaCu}_2\text{O}_{8+\delta}$, and Nd_2CuO_4 , with particular focus on the screening response to core-hole creation in the $\text{Cu-}2p_{3/2}$ level. The influence of the apex positions on the shape of the so-called main line is investigated, and found to be weak. Additionally, an Anderson impurity model was used to fit the shape of the main lines, obtaining good agreement with the data from Nd_2CuO_4 . For the other compounds, while the energy spread of the two screening channels (local and nonlocal) is well reproduced, the theory underestimates the width of the nonlocally screened feature. The shapes of the main lines are discussed in detail.

DOI: 10.1103/PhysRevB.66.024519

PACS number(s): 74.72.Jt

I. INTRODUCTION

The investigation of core level photoemission spectra can provide valuable insight into the electronic structure of materials and especially of correlated systems such as the cuprates. Although the core electrons are chemically inactive, the creation of a core hole causes a response of the valence electron system which is visible in the core level spectra. Since the discovery of the high-temperature superconductivity in the cuprate systems in 1986,¹ this technique has often been used to determine electronic parameters such as the charge transfer energy Δ for various cuprate compounds.²⁻⁴

In divalent copper compounds such as the undoped parent compounds of the high-temperature superconductors (HTSC's), copper has the electronic configuration $\text{Cu}^{2+} : [\text{Ar}] 3d^9$. This means there is a single hole in the $3d_{x^2-y^2}$ orbital per copper atom. The on-site Coulomb repulsion, described by the Hubbard parameter U ($\sim 8-9$ eV), causes localization of the holes and gives an insulating, and usually antiferromagnetic ground state for the undoped two-

dimensional cuprates. Creating a core hole in the $\text{Cu-}2p$ orbital pulls the $\text{Cu-}3d$ levels down in energy and enables a charge transfer from the surrounding ligand orbitals (in this case the $\text{O-}2p$ levels). Thus, each spin-orbit component of the $\text{Cu-}2p$ core level line in photoemission of the divalent cuprates is split into a so-called satellite line with the final state configuration $c^{-1}3d^9$ and a so-called main line with a configuration $c^{-1}3d^{10}L^{-1}$. Here c^{-1} stands for the hole in the core level and L^{-1} for a "ligand" hole in the surrounding $\text{O-}2p$ levels. In the latter final state a charge transfer process has taken place from oxygen to copper as a screening response to the core hole. This process is energetically favorable due to the large Coulomb repulsion U_{dc} between holes in the $\text{Cu-}2p$ and $-3d$ levels, thus the main line appears some 8–9 eV below the satellite on a binding energy scale.

The intensity ratio between satellite and main line and the energy separation between them are, in cluster models, related to the electronic parameters U_{dc} , Δ , and T_{pd} , the latter being the total hybridization between the $\text{Cu-}3d$ and the $\text{O-}2p$ orbitals.^{5,2,3} Δ is defined by $\Delta = \epsilon_d - \epsilon_p$, where ϵ_d and

ε_p are the energies of the Cu- $3d$ and O- $2p$ levels. Further information can be gained from the spectra by investigating the fine structure of the lines. The fine structure in the satellite is due to multiplets resulting from the interaction between the angular momenta of the core hole and the $3d$ hole in the final state. The main line shows no multiplet structure because the $3d$ shell is essentially filled. However, the fine structure of the main line is an issue of ongoing discussion. First measurements with moderate resolution carried out on polycrystalline samples led to the observation of asymmetric, broad main lines,^{2,6} which was explained in terms of the valence electronic structure,⁷ since the charge transfer is essentially the transfer of an electron from the valence band to the copper $3d$ level. Later the notions of local and nonlocal screening channels were established.^{8,9} In this picture, the local screening channel should be situated at the high binding energy side of the main line and is due to a charge transfer from the O- $2p$ orbitals next to the core-ionized copper atom—i.e., this screening response takes place on a single CuO_4 plaquette. The nonlocal screening channel is then due to further delocalization of the hole density to neighboring plaquettes, where it forms a Zhang-Rice singlet, coupling to the spin of the intrinsic $3d$ hole at the non-core-ionized copper sites. Because of the total energy reduction due to this stable spin configuration this final state is situated at the low binding energy side of the main line. Recently Karlsson *et al.*¹⁰ showed that the broadening of the main line is not per se related to the formation of Zhang-Rice singlets but to the possibility of a nonlocal screening process involving a valence band of finite width. To explain the different widths of the main lines in $\text{Bi}_2\text{Sr}_2\text{CaCu}_2\text{O}_{8+\delta}$ and in Nd_2CuO_4 the idea of a further screening channel involving the apex positions has been suggested.¹¹

Subsequent high-resolution experiments^{12,13} revealed a clear and systematic dimensionality dependence of the fine structure in the main line. The “dimensionality” of the copper-oxygen network here is defined in terms of the network formed by joining the paths with a strong superexchange interaction.^{12,13} If the Cu-O plaquettes are connected by their edges, as in Li_2CuO_2 , the Cu-O-Cu interaction is via an angle of 90° and is thus weak, giving what can be called a “zero-dimensional” network. If the CuO_4 plaquettes are connected via their corners to form a chain, as is the case in Sr_2CuO_3 , the Cu-O-Cu angle is 180° (Ref. 14) and the superexchange interaction is strong and antiferromagnetic. Connecting the plaquettes via their corners in two orthogonal directions results in a two-dimensional network.

In experiment a narrow, single component main line was observed for zero-dimensional cuprates such as Li_2CuO_2 ,^{13,15} while the main line of one-dimensional cuprates was clearly comprised of two components.¹² The single component main line for zero-dimensional cuprates is due wholly to a locally screened channel: nonlocal screening channels are impossible in this case due to the weak interaction between the Cu-O plaquettes. The two components in the main line of the one-dimensional cuprates are due to a local and a nonlocal screening channel. Several theoretical approaches have been able to describe satisfactorily the spec-

tra of zero-dimensional and one-dimensional cuprates, but have failed to describe the data from the two-dimensional cuprate $\text{Sr}_2\text{CuO}_2\text{Cl}_2$ correctly.^{10,16,17} The main line of this compound is comprised of two components, whereby the leading structure is very broad. The theories, however, predict this low-energy component to be rather narrow. However, the Cu- $2p$ data from the two-dimensional cuprate $\text{Ba}_2\text{Cu}_3\text{O}_4\text{Cl}_2$ (which has a Cu_3O_4 plane built up of interpenetrating 2D Cu_AO_2 and 0D Cu_B networks) could be described correctly within the Anderson impurity model (AIM).^{10,39} Encouraged by this we applied an AIM to fit the spectra rather than a cluster model. Although cluster models are somewhat more ostensive in their description of the physical process they are limited to finite size structures with relatively few atoms. They appear to have more problems in explaining the experimental results than the AIM.

The Cu- $2p$ core level spectra of the two-dimensional cuprates with their special importance in the context of high-temperature superconductivity are not fully understood and further investigations are clearly needed.

To clarify whether $\text{Sr}_2\text{CuO}_2\text{Cl}_2$ is a special case for the divalent two-dimensional cuprates, we have investigated single crystals of the structurally closely related compound $\text{Ca}_2\text{CuO}_2\text{Cl}_2$. Furthermore, to evaluate a possible influence of the apex positions on the shape of the spectra we have also studied single crystals of $\text{Sr}_2\text{CuO}_2\text{Br}_2$ and Nd_2CuO_4 . In the former, the apex position is occupied by another atom (Br) with respect to the case in $\text{Sr}_2\text{CuO}_2\text{Cl}_2$ (Cl), and in the T' crystal structure of Nd_2CuO_4 no apex atoms occur. To examine the influence of doping the CuO_2 plane with holes, and to relate the previously mentioned measurements of undoped, nonsuperconducting cuprates to the high-temperature superconductors themselves, we also present data from single crystals of $\text{Bi}_2\text{Sr}_2\text{CaCu}_2\text{O}_{8+\delta}$. The amount of surface contaminations was examined and found to be small, making any impact on the Cu- $2p$ photoemission spectra and conclusions drawn from them very unlikely. The experimental data have been analyzed within the framework of an Anderson impurity model. The goal of this joint experimental and theoretical investigation of two-dimensional cuprates is to determine and understand the typical situation for the two-dimensional cuprates, as has been successfully carried out in the zero- and one-dimensional cases.^{10,12,17}

The organization of the paper is as follows. In Sec. II we describe the experimental details. In Sec. III some important crystal properties of the measured compounds are collected. In Sec. IV our theoretical approach is described. Section V is devoted to the presentation of our experimental and theoretical results, which are then discussed in Sec. VI. Section VII is a summary.

II. EXPERIMENTAL

The x-ray-photoemission experiments were performed using a commercial XPS-spectrometer.¹⁸ Monochromatized Al $K\alpha$ radiation with an energy of $h\nu=1486.6$ eV and bandwidth of 0.4 eV was used as an excitation source. All measurements were carried out at room temperature. The pressure in the main chamber during the measurements was

between 1.3×10^{-8} and 6.5×10^{-8} Pa. The overall energy resolution of the measurements, estimated using the 10–90% width of the Fermi edge of gold, was 0.4 eV for an analyzer pass energy of 5.8 eV. For the calibration of the binding energy (BE) scale we used the Fermi edges of Ar ion etched gold, copper and silver metal foils (all set as zero BE) as well as the BE's of the Au $4f_{5/2}$ (84.0 eV) and Ag $3d_{3/2}$ (368.25 eV) core level lines.

Single crystals of $\text{Sr}_2\text{CuO}_2\text{Cl}_2$, $\text{Sr}_2\text{CuO}_2\text{Br}_2$, $\text{Ca}_2\text{CuO}_2\text{Cl}_2$, $\text{Bi}_2\text{Sr}_2\text{CaCu}_2\text{O}_{8+\delta}$, and Nd_2CuO_4 were mounted on sample holders using conducting epoxy and a cleavage lever was glued on top of the crystals. The crystals were cleaved in the preparation chamber ($p \sim 1 \times 10^{-7}$ Pa) by knocking off the cleavage lever. For the Nd_2CuO_4 crystals an additional cleavage technique was used, whereby a notch was sawn into the crystals and they were mounted using Ta wire. The whole sample mounting process was carried out in an argon-filled glove box for $\text{Sr}_2\text{CuO}_2\text{Br}_2$ and $\text{Ca}_2\text{CuO}_2\text{Cl}_2$ because of the strong hygroscopic behavior of these systems. The transport of the prepared samples to the spectrometer in air and their pump down took maximally two minutes. The $\text{Sr}_2\text{CuO}_2\text{Cl}_2$, $\text{Sr}_2\text{CuO}_2\text{Br}_2$, $\text{Ca}_2\text{CuO}_2\text{Cl}_2$, and $\text{Bi}_2\text{Sr}_2\text{CaCu}_2\text{O}_{8+\delta}$ samples cleaved easily, providing flat, reflecting and clean sample surfaces, all displaying remarkable inertness. Weak carbon contamination peaks appeared only after several days of measurement. The cleavage of Nd_2CuO_4 is complicated by the hardness of the material. Several attempts using the top-post method described above were required to succeed in cleaving the crystal. The surface thus produced tended to pollute faster and was not completely contamination-free, even immediately after cleavage as will be shown below.

As many of these systems are insulators, one needs to be aware of the possibility of charging during the experiment. Strong charging effects were only observed for $\text{Sr}_2\text{CuO}_2\text{Br}_2$, which resulted in a shift and deformation of the spectral features. Thus, in this case a low-energy electron flood gun was used during the measurement. Slight shifts of the spectral features were sometimes visible in the insulators $\text{Sr}_2\text{CuO}_2\text{Cl}_2$ and Nd_2CuO_4 too, but no deformation or broadening of the spectra was observed. $\text{Ca}_2\text{CuO}_2\text{Cl}_2$ and $\text{Bi}_2\text{Sr}_2\text{CaCu}_2\text{O}_{8+\delta}$ never showed any sign of charging effects. All spectra were taken at an angle of approximately 45° between the sample surface normal and the analyzer direction and a Shirley background was subtracted from the data.

III. CRYSTAL STRUCTURES

$\text{Sr}_2\text{CuO}_2\text{Cl}_2$, $\text{Sr}_2\text{CuO}_2\text{Br}_2$, and $\text{Ca}_2\text{CuO}_2\text{Cl}_2$ crystallize in the body centered, tetragonal K_2NiF_4 structure where the apex positions are occupied by Cl or Br (see Fig. 1).¹⁹ Table I provides the lattice parameters and relevant bond lengths of the compounds measured. Due to the smaller size of the Ca ion with respect to Sr, the Cu-O distance in $\text{Ca}_2\text{CuO}_2\text{Cl}_2$ is smaller than in $\text{Sr}_2\text{CuO}_2\text{Cl}_2$. The Cu-apex distance is the largest for $\text{Sr}_2\text{CuO}_2\text{Br}_2$ due to the large size of the Br ion.

Nd_2CuO_4 crystallizes in a T' structure without an apex position (see Fig. 1).²⁰ $\text{Bi}_2\text{Sr}_2\text{CaCu}_2\text{O}_{8+\delta}$ has two CuO_2

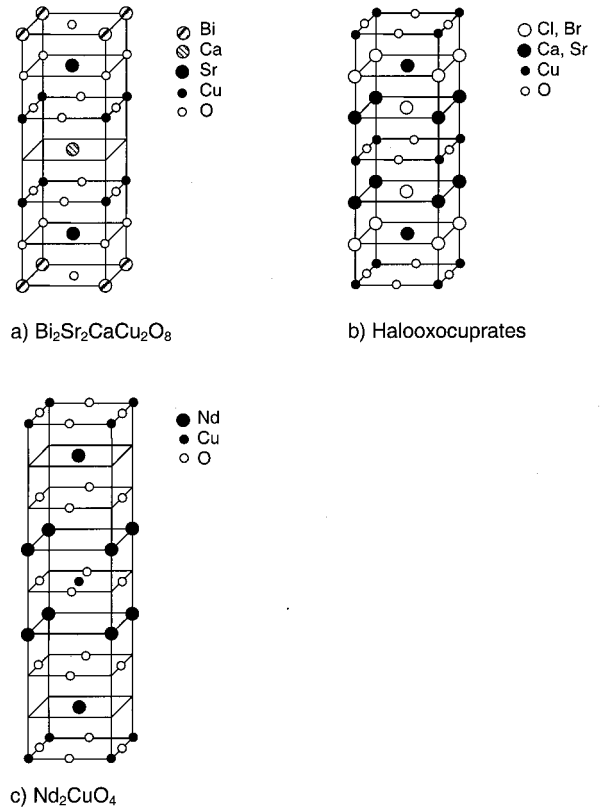


FIG. 1. Crystal structures of (a) $\text{Bi}_2\text{Sr}_2\text{CaCu}_2\text{O}_{8+\delta}$, (b) the halooxocuprates, and (c) Nd_2CuO_4 .

planes per unit cell, which are separated by Ca atoms. The oxygen atoms of the Sr-O layer form the apex position of the copper, thus only one apex position per copper atom is occupied giving a CuO_5 square-based pyramid. Our $\text{Bi}_2\text{Sr}_2\text{CaCu}_2\text{O}_{8+\delta}$ samples showed a superconducting phase transition at 87 K and are therefore relatively close to optimal doping.²¹ All the Cu-O planes of the cuprates under consideration contain a two-dimensional CuO_2 network.

IV. THEORY

The core level spectra were calculated using an Anderson impurity model (AIM). The Cu-3d orbitals of the core hole plaquette are treated separately (as an “impurity”) from the rest of the Cu-O (host) network, the latter being treated within the local density approximation (LDA). The AIM is represented by the Hamiltonian²²

$$H = \sum_{\nu=1}^{10} \left\{ \int \varepsilon \Psi_{\varepsilon\nu}^+ \Psi_{\varepsilon\nu} d\varepsilon + [\varepsilon_d - U_{dc}(1-n_c)] \Psi_{\nu}^+ \Psi_{\nu} + \int [V_{\nu}(\varepsilon) \Psi_{\nu}^+ \Psi_{\varepsilon\nu} + \text{H.c.}] d\varepsilon \right\} + U \sum_{\nu < \mu} n_{\nu} n_{\mu}, \quad (1)$$

where ε_d is the energy of the Cu-3d level and ε is the energy of the hopping electron. ν is a combined spin and orbital index. The host valence states are labeled by the energy ε and ν and the impurity Cu-3d states are labeled by ν . $\Psi_{\varepsilon\nu}$ is

TABLE I. Lattice parameters and crystal structure data for the compounds concerned.

	Lattice constants (Å)		Bond lengths (Å)		Source
	<i>a</i>	<i>c</i>	Cu-O	Cu apex	
Sr ₂ CuO ₂ Cl ₂	3.97	15.61	1.99	2.86	(Ref. 40)
Ca ₂ CuO ₂ Cl ₂	3.87	14.98	1.93	2.73	(Ref. 41)
Sr ₂ CuO ₂ Br ₂	3.99	17.16	2.0	2.98	(Ref. 42)
Nd ₂ CuO ₄	3.94	12.15	1.97		(Ref. 43)
Bi ₂ Sr ₂ CaCu ₂ O _{8+δ}	5.4	30.7	1.91	2.2	(Ref. 44)

an annihilation operator, which removes one electron from the host level. Ψ_ν annihilates one electron from an impurity Cu-3*d* level. The impurity level is pulled down from an energy of ε_d to $\varepsilon_d - U_{dc}$ when a core hole is created. The electrons in the impurity Cu-3*d* levels experience the Coulomb energy U . In this approach we explicitly treat correlation effects at the Cu impurity, while the correlation effects in the host are treated approximately at the level of the LDA. As energy zero we use the energy $\varepsilon_F = 0$, of the highest occupied state.

The idea here is to find the energy dependence of the electronic transitions from the host to the impurity in the presence of a core hole at the impurity site. First one has to calculate the local density of states (LDOS) $\rho_\nu(\varepsilon)$ of the Cu-3*d* orbitals for all compounds, with the label ν standing for the particular Cu-3*d* orbital under consideration. For this, the LMTO method was used.^{23,37} In principle, the DOS or the band structure is a result of the quantum-mechanical interaction between the orbitals, represented as a hopping. Thus, one can derive the hopping matrix elements $V_\nu(\varepsilon)$ from the LDOS using the relationship²⁴

$$\pi|V_\nu(\varepsilon)| = -\text{Im}\left\{\left[\int \frac{\rho_\nu(\varepsilon')}{\varepsilon - \varepsilon' - i0} d\varepsilon'\right]^{-1}\right\}. \quad (2)$$

We express the ground state in terms of a many-electron basis set, as indicated schematically in Fig. 2. In the simplest approximation, we use the states illustrated in Figs. 2(a) and 2(c), which describe the impurity in a d^9 configuration and in a d^{10} configuration with a hole in the valence band $d^{10}L^{-1}$. Thus we write the ground-state as²⁵

$$|E_0\rangle = A\left(\Psi_\nu|d^{10}\rangle + \int_{\varepsilon_f} a_\nu(\varepsilon)\Psi_{\varepsilon\nu}|d^{10}\rangle d\varepsilon\right), \quad (3)$$

where A is a normalization constant. The first term corresponds to a $3d^9$ configuration and the second term to a Cu $3d^{10}L^{-1}$ configuration, where L^{-1} represents one hole in a host level. Due to the various energies and the different hopping possibilities of the host levels this component is a summation over the energies of the host levels up to the Fermi energy with weights $a_\nu(\varepsilon)$. These weighing factors are given by¹⁰

$$a_\nu(\varepsilon) = \frac{V_\nu(\varepsilon)}{\Delta E - \varepsilon_d + \varepsilon}, \quad (4)$$

whereby ΔE is the lowering of total energy of the system caused by hybridization of the mixed ground state relative to the energy of the pure $3d^9$ state. The expression in Eq. (3) is useful for qualitative discussions but it does not give very accurate results. In our numerical calculations we therefore also include the states shown as (b) and (d) in Fig. 2.

The core level spectra are calculated using a resolvent operator and inserting intermediate states similar to the two terms in Eq. (3).^{22,25} ε_d is used as an adjustable parameter to fit the model spectra to the experimental intensity ratio between satellite and main line I_S/I_M .

In the presence of a core hole, the $d^{10}L^{-1}$ states are substantially lower in energy than the d^9 states. For a qualitative discussion (but not in the calculations), we therefore neglect the hopping between these states in the presence of a core hole. We then obtain the simplified spectrum¹⁰

$$\rho = A^2[a^2(\varepsilon)\Theta(-\varepsilon) + \delta(\varepsilon - \varepsilon_d + U_{dc})]. \quad (5)$$

The first term corresponds to the main line and describes how an electron has hopped from the valence band into the

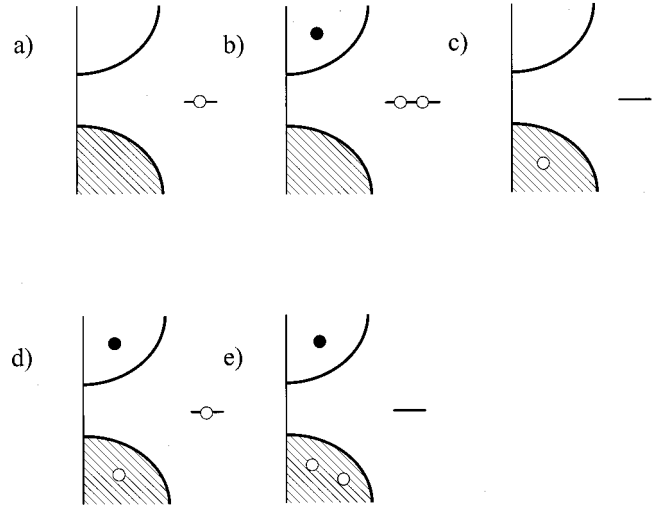


FIG. 2. Basis states for divalent Cu. (a) Describes a Cu d^9 configuration. (b) Shows the result of a hop of a 3*d* electron into the conduction band. In (c), a valence electron has hopped into the 3*d* level. If a valence electron hops into the conduction band we arrive at (d) and in state (e) one valence electron has hopped in the conduction band and another into the 3*d* level.

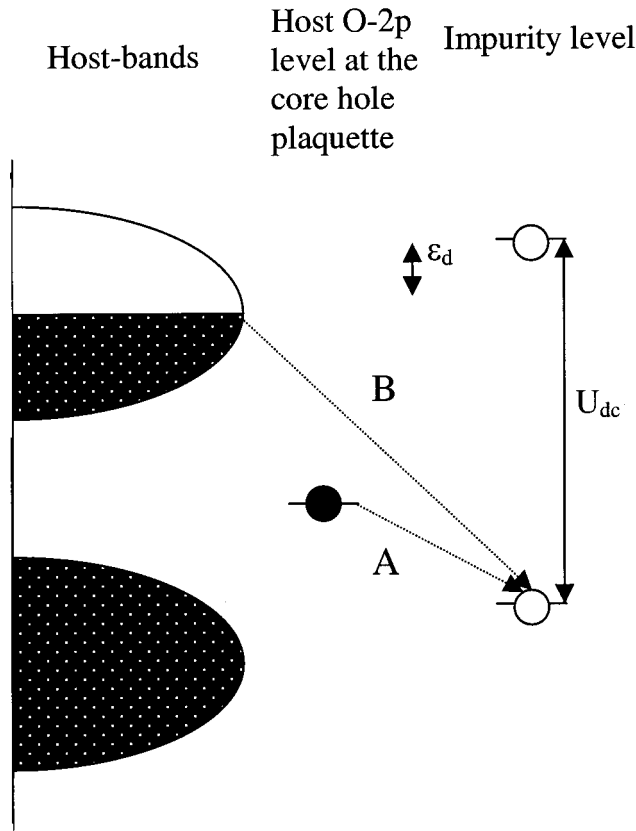


FIG. 3. Schematic representation of charge transfer in the AIM. The Cu-3*d* impurity level is shown on the right side of the figure, whereby its energy has been lowered in the presence of the core hole by U_{dc} . Charge transfer to the Cu-3*d* impurity either occurs from the nonbonding oxygen orbitals from the core ionized plaquette (center of the picture, arrow A) or from the antibonding host bands (left side of the picture, arrow B).

Cu-3*d* level to screen the core hole. The second term describes the satellite, where such a screening has not taken place.

The most important energy bands in the cuprates studied here consist of antibonding and bonding combinations of the $3d_{x^2-y^2}$ Cu orbital with O-2*p* orbitals on the neighboring four O sites. When the Cu core hole is created and the Cu-3*d* level is pulled down, the O-2*p* orbitals pointing towards the core ionized Cu atom form a nonbonding combination. An electron from this level can hop into the Cu-3*d* level to screen the core hole. The corresponding structure in the spectrum is usually referred to as the locally screened peak. Alternatively, the core hole can be screened by an electron hopping into the Cu-3*d* level from the antibonding band in the host surrounding the core ionized atom. The corresponding structure in the spectra is referred to as the nonlocally screened feature. These hopping processes in the presence of the core hole are shown schematically in Fig. 3.

As can be seen from Eq. (5), the weight of the different structures is determined by $a_\nu(\epsilon)$ in Eq. (4). This depends on the hopping matrix elements between the host and the Cu-3*d* level and, in particular, on the energy denominator. This denominator has the effect of strongly favoring hopping from

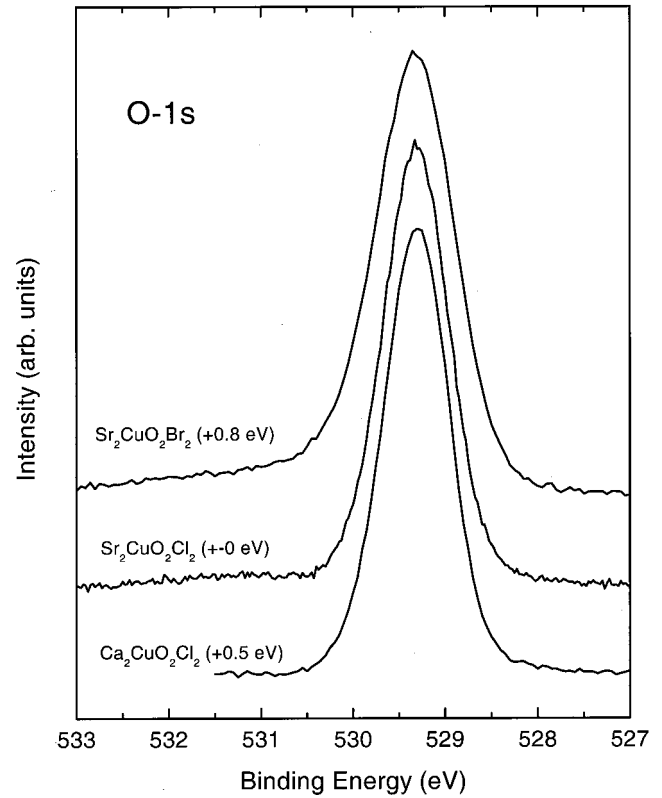


FIG. 4. O-1*s* core level photoemission spectra of $\text{Sr}_2\text{CuO}_2\text{Cl}_2$, $\text{Ca}_2\text{CuO}_2\text{Cl}_2$, and $\text{Sr}_2\text{CuO}_2\text{Br}_2$. The numbers in brackets indicate the quantity and direction by which the spectra have been shifted in energy to align them with that of $\text{Sr}_2\text{CuO}_2\text{Cl}_2$.

the highest occupied states. This is in particular the case if $\Delta E - \epsilon_d$ is small, since $a_\nu(\epsilon)$ then drops very quickly as epsilon becomes more negative.

V. RESULTS

A. Experiment

1. Halooxocuprates

Figure 4 shows the O-1*s* core level spectra of $\text{Sr}_2\text{CuO}_2\text{Cl}_2$, $\text{Sr}_2\text{CuO}_2\text{Br}_2$, and $\text{Ca}_2\text{CuO}_2\text{Cl}_2$. For comparison, the spectra of $\text{Sr}_2\text{CuO}_2\text{Br}_2$ and $\text{Ca}_2\text{CuO}_2\text{Cl}_2$ have been aligned to the $\text{Sr}_2\text{CuO}_2\text{Cl}_2$ line (the energy shifts are as indicated in the figure). The original positions of the O-1*s* lines were 528.3 eV for $\text{Sr}_2\text{CuO}_2\text{Br}_2$ and 528.8 eV for $\text{Ca}_2\text{CuO}_2\text{Cl}_2$. The measured spectrum of $\text{Sr}_2\text{CuO}_2\text{Br}_2$ appeared at lower binding energies most likely because of the use of the flood gun. The downward shift in the case of $\text{Ca}_2\text{CuO}_2\text{Cl}_2$ may be due to a different position of the chemical potential in the gap with respect to $\text{Sr}_2\text{CuO}_2\text{Cl}_2$, since all lines of the former are slightly shifted to lower binding energies. The O-1*s* binding energy of $\text{Sr}_2\text{CuO}_2\text{Cl}_2$ measured here is about 529.3 eV, consistent with previous measurements.¹² The full width at half maximum (FWHM) of the O-1*s* spectra of $\text{Sr}_2\text{CuO}_2\text{Cl}_2$ and $\text{Ca}_2\text{CuO}_2\text{Cl}_2$ are both 0.8 eV indicating single component lines. The FWHM of $\text{Sr}_2\text{CuO}_2\text{Br}_2$ is slightly broader at 1 eV, which is probably

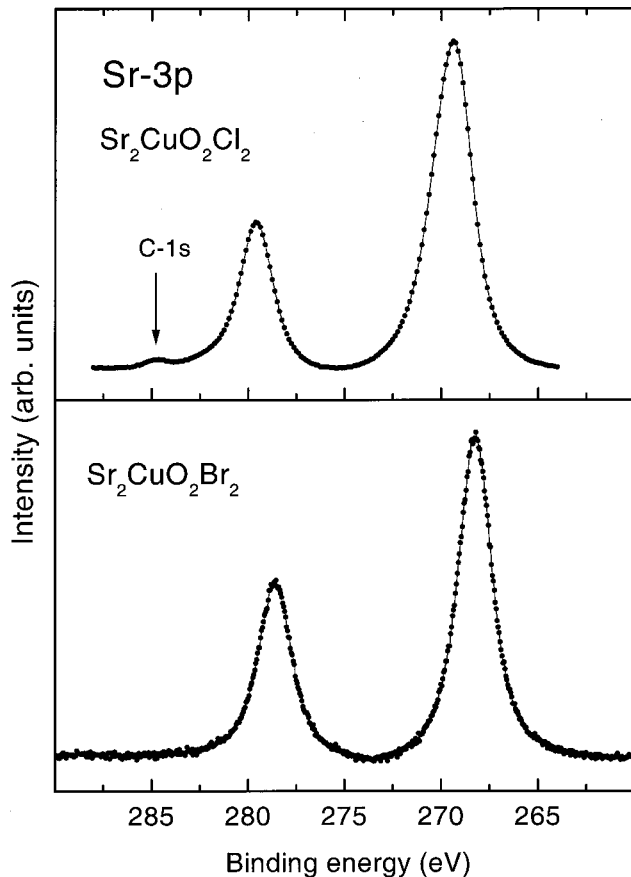


FIG. 5. Sr-3*p*/C-1*s* core level spectra of $\text{Sr}_2\text{CuO}_2\text{Cl}_2$ and $\text{Sr}_2\text{CuO}_2\text{Br}_2$.

due to the use of the flood gun. We assume a single component line for the $\text{Sr}_2\text{CuO}_2\text{Br}_2$ as well. No contamination is visible in any of the spectra, which would appear as an additional component at the higher-binding-energy side of the peak.

Figure 5 illustrates the cleanliness of the sample surfaces as concerns possible adventitious carbon or carbonate contamination, which would occur at binding energies of around 285 eV for carbon and of 288–290 eV for carbonate contamination. The complete absence of a C-1*s* signal in the case of $\text{Sr}_2\text{CuO}_2\text{Br}_2$ indicates that the sample surface is completely free of carbon contamination. For $\text{Sr}_2\text{CuO}_2\text{Cl}_2$ and $\text{Ca}_2\text{CuO}_2\text{Cl}_2$, only weak C-1*s* spectral features develop after long measuring times. The cross section corrected intensity ratios of the C-1*s* to the O-1*s* signals for $\text{Sr}_2\text{CuO}_2\text{Cl}_2$ and $\text{Ca}_2\text{CuO}_2\text{Cl}_2$ are 0.04 and 0.08, respectively. This corresponds to relative atomic carbon contamination ratio at the surface of around 1.3% for $\text{Sr}_2\text{CuO}_2\text{Cl}_2$ and 2.3% for $\text{Ca}_2\text{CuO}_2\text{Cl}_2$. Therefore, from the O-1*s* and C-1*s* spectra we can conclude that the halooxocuprate cleavage surfaces are almost completely free of extrinsic contamination. Furthermore the CuO_2 layers are not at the surface after cleavage and thus the minimal carbon quantities observed don't have an important effect on the copper spectra.

Figure 6 shows the Ca-2*p* core level spectrum of $\text{Ca}_2\text{CuO}_2\text{Cl}_2$. Although the sample was almost contamination-free and there is formally only a single crys-

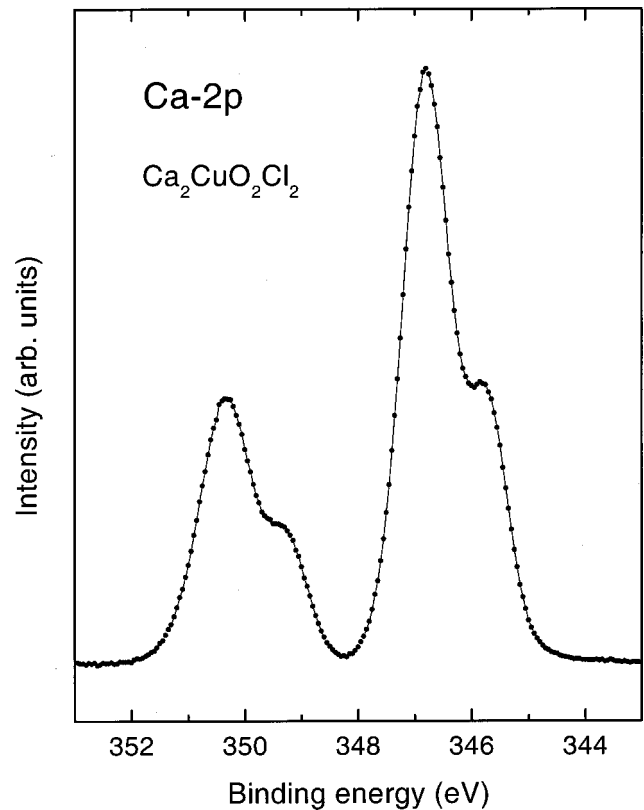


FIG. 6. Ca-2*p* core level spectrum of $\text{Ca}_2\text{CuO}_2\text{Cl}_2$. Note that, the spectrum consists of a pair of spin-orbit split doublets.

tallographically unique calcium site in the lattice, the spectrum consists of a pair of spin orbit split doublets. Similar splittings have been detected earlier for other Ca-containing cuprates.⁴⁵ Since $\text{Ca}_2\text{CuO}_2\text{Cl}_2$ does not show any signs of oxygen-containing contamination in the O-1*s* spectra, practically the only possibility to explain this feature in terms of contamination would be by the presence of a carbide-like compound at the surface. This would be in contradiction to the binding energies observed for both carbon and calcium, thus ruling out this possibility. Furthermore, no second component was found in the chlorine lines and no similar feature was found for the Sr core level lines in the isostructural system $\text{Sr}_2\text{CuO}_2\text{Cl}_2$. Neutron-diffraction measurements of $\text{Ca}_2\text{CuO}_2\text{Cl}_2$ did not show any signs of a lowered crystal symmetry²⁶ in these crystals. The binding energy separation between the doublets is around 1 eV and their intensity ratio is around 1:3. A quantitative analysis shows that the cross-section corrected ratio between the calcium and chlorine 2*p* signals is 1:1 (as expected from the stoichiometry) if one considers both Ca components. Thus, no calcium excess is present in the Ca-Cl block layers. In the Ca-2*p* spectra of $\text{Bi}_2\text{Sr}_2\text{CaCu}_2\text{O}_{8+\delta}$ (not shown), a small shoulder is also observable, but in this case it is explained by a certain fraction of calcium atoms that occupy the crystallographic sites of the chemically similar Sr atoms.²⁷ Such a process is not possible in $\text{Ca}_2\text{CuO}_2\text{Cl}_2$ because of the absence of Sr sites. Nevertheless, Ca is a light and small ion and thus the Ca sublattice may be prone to disorder in the crystal structure. We suggest this to be a possible explanation for the observed splitting of

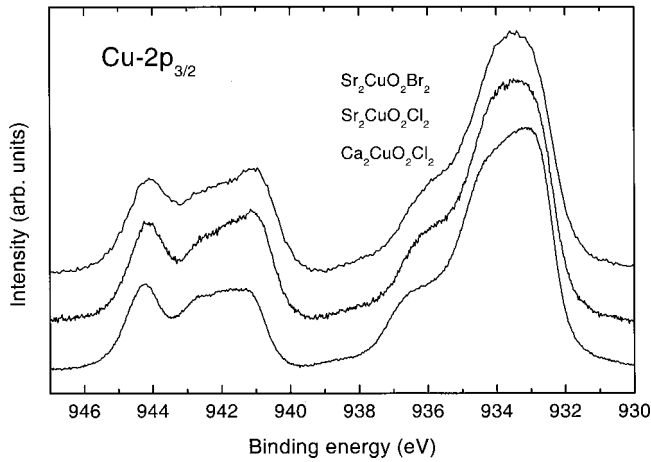


FIG. 7. Cu- $2p_{3/2}$ spectra of the halooxocuprates $\text{Sr}_2\text{CuO}_2\text{Br}_2$, $\text{Sr}_2\text{CuO}_2\text{Cl}_2$, and $\text{Ca}_2\text{CuO}_2\text{Cl}_2$. The spectra are aligned in energy such that the respective O- $1s$ binding energies line up with those of $\text{Sr}_2\text{CuO}_2\text{Cl}_2$. The spectra are normalized to the maximum.

the Ca- $2p$ core level line in $\text{Ca}_2\text{CuO}_2\text{Cl}_2$ and the absence of this feature for Sr in $\text{Sr}_2\text{CuO}_2\text{Cl}_2$, which is in agreement with conclusions drawn for other Ca-containing cuprates.⁴⁵ In this context we mention that $\text{Ca}_2\text{CuO}_2\text{Cl}_2$ is much more easy to dope chemically than $\text{Sr}_2\text{CuO}_2\text{Cl}_2$.^{28,29} It is natural to assume that the component due to the disordered Ca gives rise to the smaller doublet, thus meaning that these Ca ions appear at lower BE values close, in fact, to those of metallic calcium.³⁰ If the BE of the disordered component were to be taken at face value in a simple initial state charging model, it could point to an alteration of the overall charge balance in the system, leading to a p -type doping of the CuO_2 planes. However, as this paper clearly shows, the final state screening response can also strongly modify core level photoemission line shapes and energies. In any case, such a Ca disorder could be an realistic explanation for the observation that $\text{Ca}_2\text{CuO}_2\text{Cl}_2$ is the only insulating halooxocuprate that never shows charging effects—even in ARPES experiments at low temperatures³¹—the reason being quite simply that the gap is not as clean as in the other systems such as $\text{Sr}_2\text{CuO}_2\text{Cl}_2$.

Figure 7 shows a comparison of the Cu $2p_{3/2}$ spectra of $\text{Sr}_2\text{CuO}_2\text{Cl}_2$, $\text{Sr}_2\text{CuO}_2\text{Br}_2$, and $\text{Ca}_2\text{CuO}_2\text{Cl}_2$. The result for $\text{Sr}_2\text{CuO}_2\text{Cl}_2$ is in agreement with previous measurements.¹² The spectra have been aligned such that the respective O- $1s$ BE's match that of $\text{Sr}_2\text{CuO}_2\text{Cl}_2$. The shape of the main line is very similar for all of these three systems: in fact the spectra of $\text{Sr}_2\text{CuO}_2\text{Cl}_2$ and $\text{Sr}_2\text{CuO}_2\text{Br}_2$ are almost identical. $\text{Ca}_2\text{CuO}_2\text{Cl}_2$ shows a smaller intensity ratio between the satellite and main line with respect to the other compounds. Table II gives the intensity ratio between the satellite and main lines, their energy separation, as well as the FWHM of the main line for all the compounds studied in this paper. Generally, one observes a broad satellite line due to the multiplet splitting between the angular momentum of the Cu- $2p$ core hole and the valence hole in the $3d$ shell. As mentioned in the Introduction, the main line is also a broad structure that can be considered to consist of two components. The shape of the main line will be discussed in detail in Sec. VI.

TABLE II. Characteristic features of the Cu $2p_{3/2}$ spectra. Despite the asymmetric shape of the main line, the FWHM still gives a measure of the width of the low-binding-energy part since the shoulder structure becomes appreciable at intensities below half of the maximum.

Material	FWHM (eV)	I_S/I_M	$E_S - E_M$ (eV)
$\text{Sr}_2\text{CuO}_2\text{Cl}_2$	2.8	0.51	8.4
$\text{Ca}_2\text{CuO}_2\text{Cl}_2$	2.9	0.38	8.6
$\text{Sr}_2\text{CuO}_2\text{Br}_2$	2.8	0.52	8.5
$\text{Bi}_2\text{Sr}_2\text{CaCu}_2\text{O}_{8+\delta}$	3.8	0.42	8.3
Nd_2CuO_4	2.2	0.32	8.9

2. $\text{Bi}_2\text{Sr}_2\text{CaCu}_2\text{O}_{8+\delta}$ and Nd_2CuO_4

Figure 8 shows the O- $1s$ and the Sr- $3p/C-1s$ spectra of $\text{Bi}_2\text{Sr}_2\text{CaCu}_2\text{O}_{8+\delta}$. These spectra prove the cleanliness of the cleavage surface. No high binding energy component is visible either in the O- $1s$ or the Sr- $3p$ spectra, and only a very weak adventitious carbon-related peak in the vicinity of 285 eV is observed in the latter. The fine structure of the O- $1s$ line is related to the different chemical environments of the oxygen atoms in the crystal: covalent Cu-O on the low binding energy side, more ionic Sr-O and Bi-O on the high-binding-energy side.³²

The O- $1s$ spectrum of Nd_2CuO_4 is depicted in Fig. 9. A clear high-binding-energy component at 531.2 eV is seen in

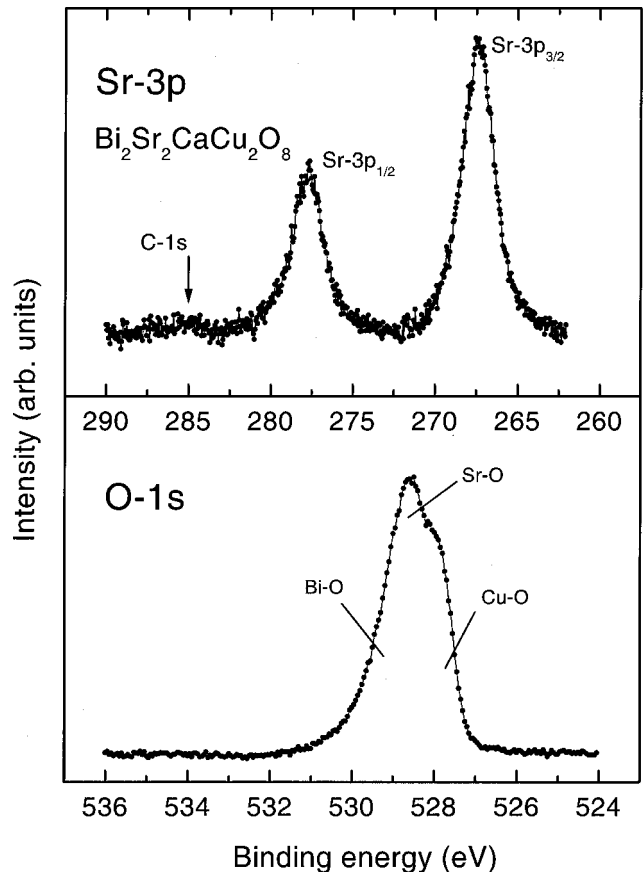


FIG. 8. O- $1s$ and Sr $3p/C-1s$ spectra of $\text{Bi}_2\text{Sr}_2\text{CaCu}_2\text{O}_{8+\delta}$ indicating the quality of the cleavage surface.

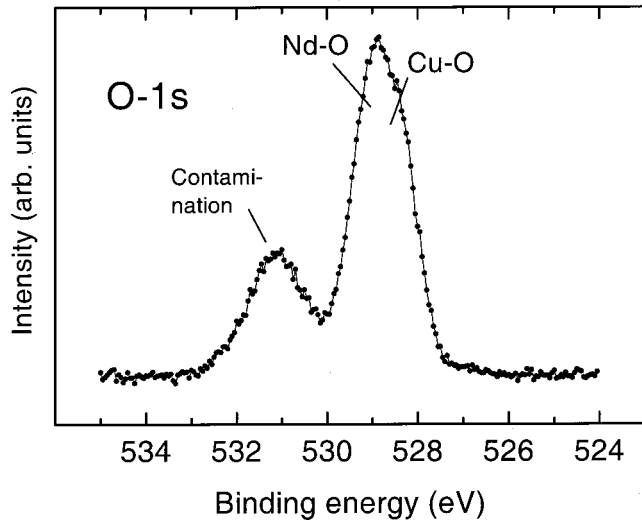


FIG. 9. O-1s spectrum of the cleavage surface of Nd_2CuO_4 . A contamination-related feature located at higher binding energy is clearly visible, as is the multicomponent nature of the O-1s main line.

the O-1s spectrum even immediately after successful cleavage of the single crystal. The same cleavage surface did exhibit adventitious carbon contamination (BE=285 eV), but it was only minimally more intense (C-1s/O-1s ratio of 0.09) than was the case for $\text{Ca}_2\text{CuO}_2\text{Cl}_2$. The crystal structure of Nd_2CuO_4 contains two different oxygen sites, which are likely to be contained in the 1.4 eV broad main line centered at 528.9 eV: again the covalent Cu-O bond on the lower-binding-energy side and the more ionic Nd-O bond on the higher-binding-energy side. The low binding energy of the carbon contamination, coupled to the low absolute C contamination level rules out a carbonate origin for the O-1s high-binding-energy (531.2 eV) component. The other core level lines could all be assigned unambiguously to Nd or Cu. Consequently, we suggest the presence of an oxide such as Nd_2O_3 located on the surface to be a possible reason for the high-binding-energy feature of the O-1s core level line. Heating the cleavage surface in UHV leads to the disappearance of the weak carbon contamination, but also to a decrease of the I_S/I_M ratio, and an increase in the oxygen high BE peak.

Figure 10 shows a comparison of the Cu-2p_{3/2} spectra of Nd_2CuO_4 , $\text{Bi}_2\text{Sr}_2\text{CaCu}_2\text{O}_{8+\delta}$, and $\text{Ca}_2\text{CuO}_2\text{Cl}_2$. No further assumptions or corrections as regards the binding energy scale were made. $\text{Bi}_2\text{Sr}_2\text{CaCu}_2\text{O}_{8+\delta}$ shows a slightly broader main line than $\text{Ca}_2\text{CuO}_2\text{Cl}_2$, but the shape is roughly the same as in the undoped halooxocuprates. In the case of the HTSC, the main line contains a weak contribution from the Bi-4s core level line ($E_B=940$ eV) but this leaves the main spectral features unaffected. In contrast to $\text{Bi}_2\text{Sr}_2\text{CaCu}_2\text{O}_{8+\delta}$, the main line of Nd_2CuO_4 is clearly narrower than those of the other systems, with a significant reduction in the prominence of the high-BE shoulder seen at 936 eV in $\text{Ca}_2\text{CuO}_2\text{Cl}_2$. In the literature different results have been reported for Nd_2CuO_4 . While low-resolution measurements on epitaxial films³³ show a considerably larger

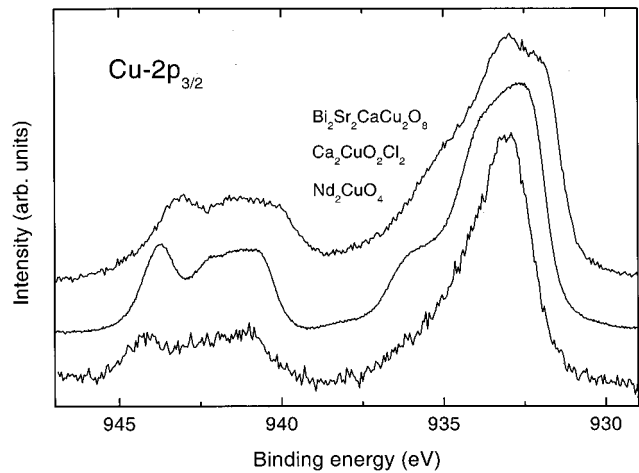


FIG. 10. Cu-2p_{3/2} core level spectra of Nd_2CuO_4 and $\text{Bi}_2\text{Sr}_2\text{CaCu}_2\text{O}_{8+\delta}$ with that of $\text{Ca}_2\text{CuO}_2\text{Cl}_2$ as a reference. The data have been normalized to have equal maximum intensity.

FWHM of 3.39 eV (here 2.2 eV), results on polycrystalline samples are roughly in agreement with our results.^{11,34,38} The intensity ratio between the satellite and main line for Nd_2CuO_4 is also the smallest for all compounds studied here (see Table II).

B. Theoretical results

Figures 11 and 12 show the results of the calculations of the Cu-2p_{3/2} main line shape within the AIM. Since the AIM describes an infinite solid, the intrinsic spectrum is continuous. However, to take into account the core-hole lifetime broadening and the instrumental resolution, the theoretical spectra have been broadened with a Lorentzian and a Gaussian, respectively. In an earlier paper⁷ some of us studied the formally 3d¹⁰ system Cu_2O , for which there is no internal source of broadening for the main peak within the present AIM theory. Experimental data from this compound were therefore used to determine the lifetime broadening contribution, which was found to be 1.1 eV (FWHM). In Fig. 11 we have used a somewhat larger lifetime (Lorentzian) broadening of 1.5 eV (FWHM), which yields better agreement with the experimental data. The increased broadening used here may simulate the effect of a further broadening mechanism missing in the theory. For the Gaussian broadening we use the instrumental resolution 0.4 eV (FWHM). Since the detailed fine structure in the calculated spectrum is blurred by the broadening, in Fig. 12 we show the spectra with reduced broadening (FWHM of 0.2 eV for both the Gaussian and Lorentzian contributions).

It is interesting to note in the experimental data that both the main line for Nd_2CuO_4 is narrower and that the high-binding-energy shoulder is weaker than for the other compounds studied here. Nd_2CuO_4 differs from these compounds by the absence of apex atoms. To explore this theoretically, we have also calculated the spectrum expected for Nd_2CuO_4 if it were to have the same crystal structure as La_2CuO_4 , by artificially moving the O atoms of Nd_2CuO_4 into the apex positions. The LDA calculation for this new

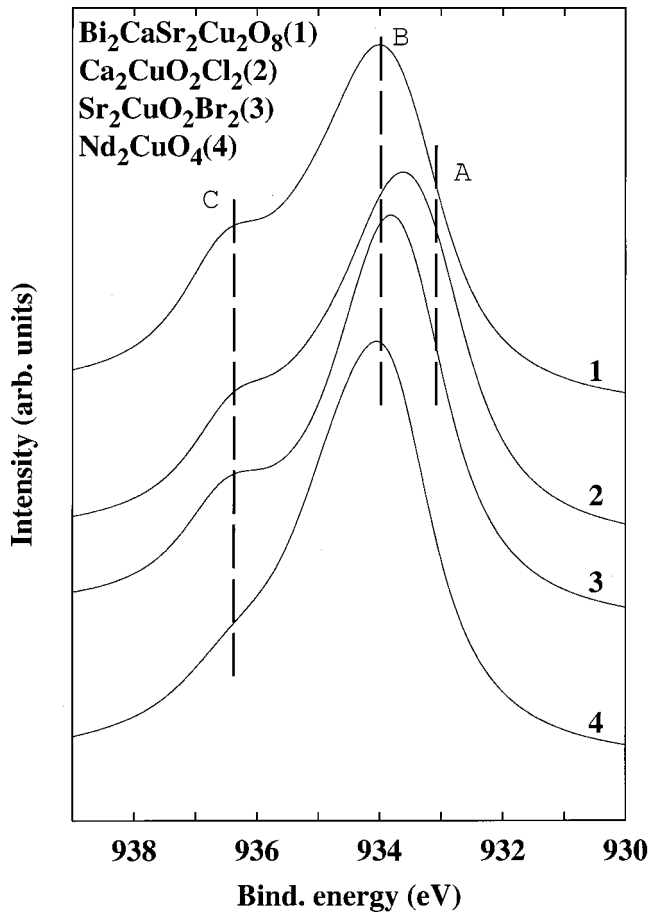


FIG. 11. Results of the AIM calculations (for details see text) of the main line of the Cu- $2p_{3/2}$ photoemission spectra. The theoretical spectra have been broadened with a Gaussian of width 0.4 eV and a Lorentzian of width 1.5 eV to account for the effects of instrumental resolution and core hole lifetime, as well as other possible broadening channels.

structure was performed in two ways. One route took the potential parameters²³ describing the atoms of Nd_2CuO_4 as they were for its true crystal structure and then calculated the band structure and the hopping matrix elements in the La_2CuO_4 structure. The second method involved the iteration of this first calculation to self-consistency, thereby allowing the potential parameters to adjust in response to the new structure. The results of the latter route are shown in Fig. 13. It is interesting to note that the calculated results for the Cu- $2p_{3/2}$ main line are not changed much by the presence or absence of O apex atoms.

VI. DISCUSSION

We now consider the shape of the Cu $2p_{3/2}$ main line spectra in detail. To ease comparison with each other and with the AIM results, we show in Fig. 14 all the experimental spectra aligned to the O- $1s$ line in each case. The energetic match-up of the components indicated A, B, and C in the spectra of the different compounds appears to be quite suggestive, but nevertheless we will focus in the following mainly on a discussion of the shape of the main lines, as this

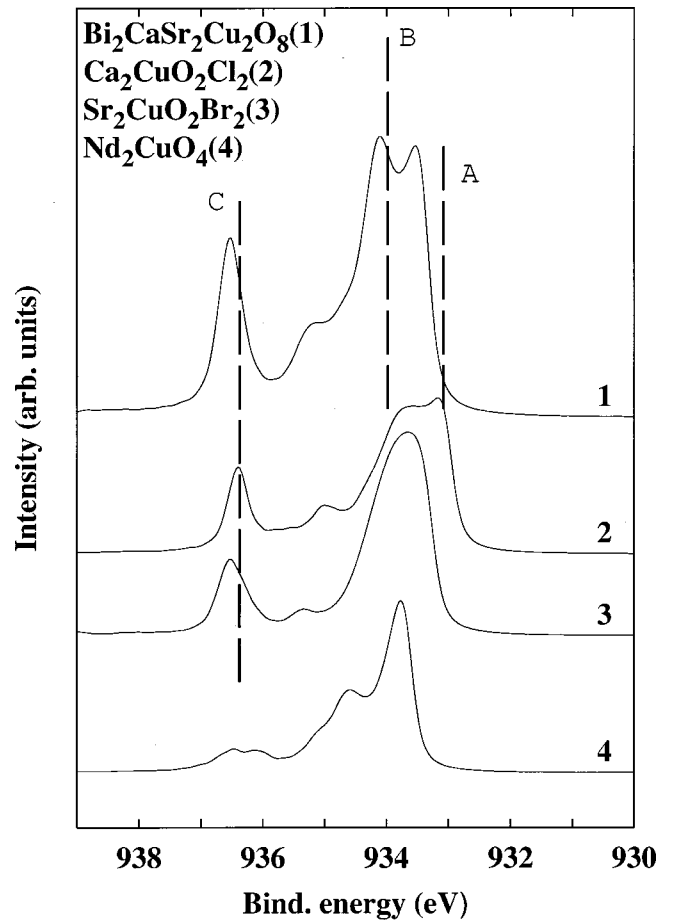


FIG. 12. Results of the AIM calculations (for details see text) for the main line of the Cu- $2p_{3/2}$ photoemission spectra in which the broadening of the theoretical spectra has been reduced (Gaussian FWHM 0.2 eV and Lorentzian FWHM 0.2 eV) to reveal the underlying fine structure.

alignment on the energy scale does not consider possible differences in the Madelung potentials in these systems, even if their influence is weak.⁶

First we consider the halooxocuprates. The main structural difference between $\text{Sr}_2\text{CuO}_2\text{Cl}_2$ and $\text{Sr}_2\text{CuO}_2\text{Br}_2$ is the identity of the apex atom, as the bond lengths in the copper oxygen network itself are nearly the same (see Table I). Comparing the Cu $2p_{3/2}$ core level spectra, one notes that the shape of the spectra, and in particular of the main lines is almost identical. This suggests that the apex position does not influence the spectra directly. This is in contradiction to the scenario proposed in Ref. 11, in which the different breadth of the main lines in La_2CuO_4 , $\text{Bi}_2\text{Sr}_2\text{CaCu}_2\text{O}_{8+\delta}$ and Nd_2CuO_4 was linked to the absence of apex atoms in Nd_2CuO_4 and the consequent impossibility of a charge transfer process from the apex oxygen. Taking the experimental evidence from the halooxocuprates and Nd_2CuO_4 together with the theoretical evidence presented in Fig. 13, we can clearly rule out a significant role for the apex atoms in the screening of Cu- $2p$ core holes in the 2D cuprates.

As mentioned earlier, to clarify how “universal” the broad shape of the Cu $2p_{3/2}$ main line is in two-dimensional CuO_2 plane systems, as well as to investigate how hole dop-

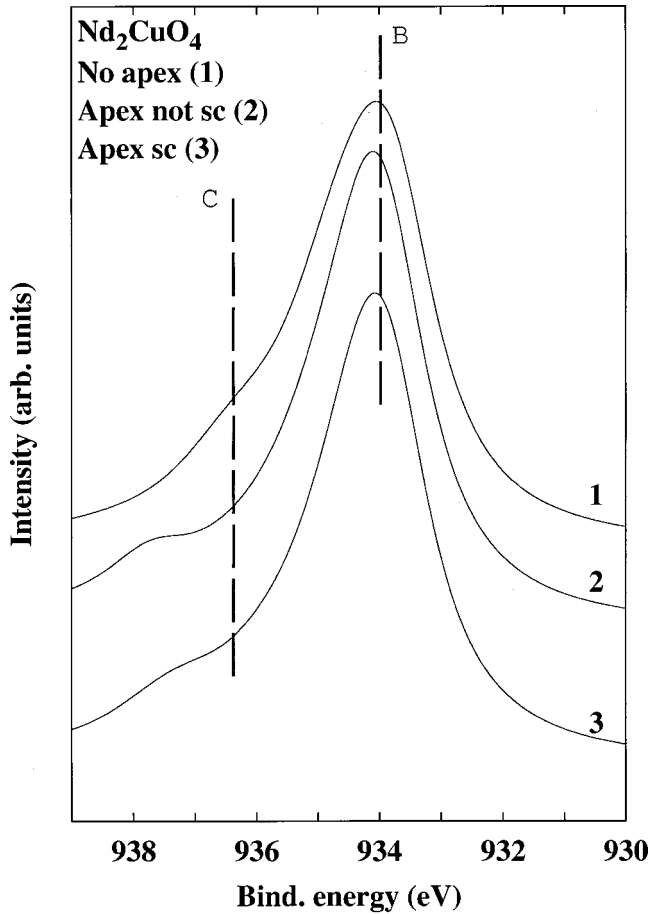


FIG. 13. AIM results for the main line Cu-2p_{3/2} spectra of Nd₂CuO₄ in its true crystal structure (1) and in the La₂CuO₄ structure using non-self-consistent (2) and self-consistent (3) potential parameters. Note that in (2) and (3) there are O apex atoms present. The results have been broadened with a 0.4 eV Gaussian and a 1.5 eV Lorentzian.

ing influences the spectra we have also investigated the well-known hole-doped superconductor Bi₂Sr₂CaCu₂O_{8+δ} and the undoped parent compound for the electron-doped superconductors Nd₂CuO₄. As can be seen in Fig. 14, the main line of Bi₂Sr₂CaCu₂O_{8+δ} is the broadest one of all the compounds studied. This may be partly related to a formal Cu³⁺ contribution due to the hole doping of the system. The Bi₂Sr₂CaCu₂O_{8+δ} data themselves are in agreement with previous measurements.^{11,35} The spectra of Nd₂CuO₄ may be influenced by the surface contamination discussed in the context of Fig. 9, but it is hard to find reasons why the main line should narrow so drastically due to a moderate O-related contamination. On the basis of the results of our AIM calculations shown in Figs. 11 and 12, we assign the components labeled A and B in Fig. 14 to the nonlocal screening channel and the weaker feature C (visible as a shoulder), to the locally screened channel. Since we consider both A and B to be the result of the same intrinsic band structure, we refer to them from now on as a single entity, which we call the leading peak. The comparison of the experimental and theoretical spectra indicates that the AIM describes the overall width of the main line spectra quite well. This width depends on the

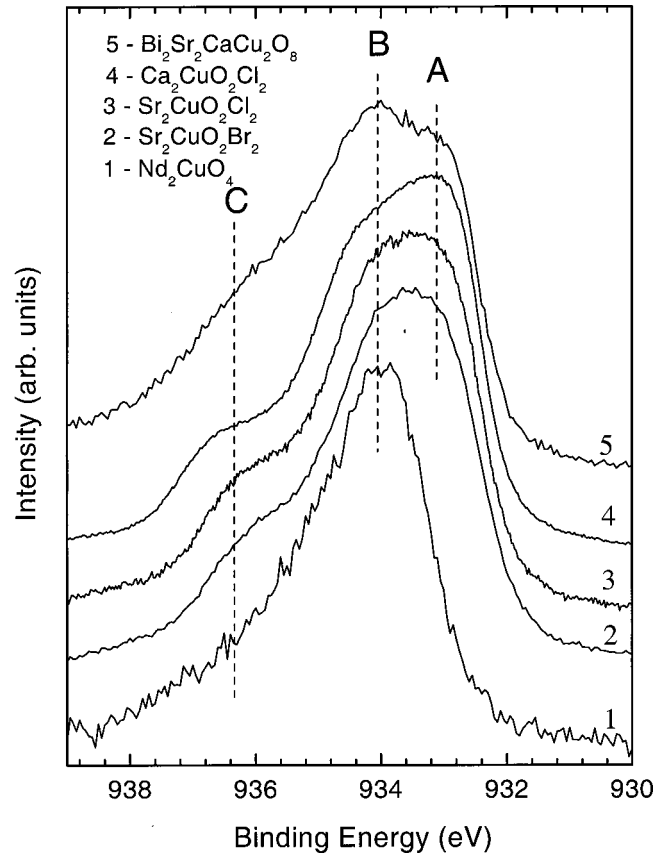


FIG. 14. Comparison of the experimental data for the Cu-2p_{3/2} main lines of all the compounds under consideration.

splitting between the local and nonlocally screened peaks, which in turn is determined by the hopping parameters obtained from the *ab initio* band structure calculations. The leading peak, ascribed above to nonlocal screening, is, however, broader and more structured in the experimental spectra than is the case in the AIM. The calculated spectra shown in Fig. 12 (with reduced broadening) illustrates that the AIM already gives a substantial width and structure to the nonlocally screened peak. In particular, the width is larger for Bi₂Sr₂CaCu₂O_{8+δ} and Ca₂CuO₂Cl₂ than for Nd₂CuO₄, in agreement with experiment. The width, however, does remain smaller than that observed in experiment and when the larger broadening is used (as in Fig. 11), very little fine structure survives in the nonlocally screened feature.

The shape of the main line of the 2D compounds measured here is quite similar in each case with the exception of Nd₂CuO₄, which differs with regard to the following points. (a) The main line as a whole covers less area and in particular the leading peak is less structured than for the other compounds. This leads to the observed absence of component A in Fig. 14. (b) The intensity ratio I_S/I_M is the smallest of all the compounds studied despite the fact that Nd₂CuO₄ does not have the smallest Cu-O bond lengths (see Table I). (c) The spectral weight of the locally screened peak (C in Fig. 14) is much weaker than for the other compounds. (d) The binding energy of the center of gravity of the main line is higher than for the other compounds.

Before discussing the implications of these observations,

we mention the possibility of an oxygen loss at surface after cleavage, which certainly takes place, for example, in the $\text{YBa}_2\text{Cu}_3\text{O}_{7-\delta}$ system. In this case, this would cause a certain formally monovalent fraction, which would naturally reduce the I_S/I_M ratio. Our observation that the shape of the main line narrows and the I_S/I_M ratio decreases upon vacuum annealing of the Nd_2CuO_4 cleavage surface would be consistent with an oxygen-loss scenario, however, it is unlikely that the pristine cleavage surface suffers the same problems.

The small I_S/I_M ratio observed for Nd_2CuO_4 has been accounted for with a very small or even negative value of Δ , implying that the Cu-3*d* level energy ε_d is lying at or below the energy of the O-2*p* related states.³⁴ This result is in quantitative disagreement with optical measurements,³⁶ which yield higher values for Δ ($\Delta = 1.5$ eV), but which do nevertheless show that Δ for Nd_2CuO_4 is significantly smaller than for other cuprates such as $\text{Sr}_2\text{CuO}_2\text{Cl}_2$.

We have first performed a simplified calculation using the ground state given in Eq. (3), i.e., including only the states (a) and (c) in Fig. 2. To describe the small experimentally observed weight of the satellite, it is also necessary to put the Cu-3*d* level at a lower energy than for the other compounds under consideration. This means that the $d^{10}L^{-1}$ configurations have more weight in the initial state, leading to a weaker (d^9) satellite in Nd_2CuO_4 . We now focus on the simplified expression [Eq. (5)] for the spectrum, which is determined by the coefficient $a_\nu(\varepsilon)$ in Eq. (4). The energy $\Delta E - \varepsilon_d$ in the denominator represents the energy lowering of the ground state relative to the lowest d^{10} configuration. Since the d^9 configuration is substantially higher in energy than the lowest $d^{10}L^{-1}$ for Nd_2CuO_4 , this energy gain is small. This leads to a large coefficient $a(\varepsilon)$ for $\varepsilon=0$, corresponding to the creation of a hole in the highest occupied state. The coefficient $a(\varepsilon)$ then drops very quickly, when ε in Eq. (3) becomes more negative. The result is that the local screening peak has a small weight. We now move on to perform a more realistic calculation, including in addition the states (b) and (d) (see Fig. 2) in the basis set. We then find that to obtain the correct weight for the satellite, $\varepsilon_d - \varepsilon_F$ should have a similar value as for the other compounds such as $\text{Sr}_2\text{CuO}_2\text{Br}_2$. This is consistent with the LDA calculations, which also find similar values for the position of the center of the Cu-3*d* band in relation to the highest occupied state. State (b) couples to state (a) and state (d) to state (c), effectively lowering the energies of the states (a) and (c). State (b), however, is higher in energy than state (d), due to the Coulomb repulsion between the two 3*d* holes in state (b). The net effect is therefore that the $d^{10}L^{-1}$ states are lowered more than the d^9 state. For Nd_2CuO_4 , the coupling to the conduction states, in particular at energies around 1–3 Ryd, is very strong compared with the other compounds studied here. In the simple calculation using just the states (a) and (c) of Fig. 2 this was simulated by using an unusually small value of $\varepsilon_d - \varepsilon_F$, while in the more complete calculation [including states (a)–(d)], we can use values of $\varepsilon_d - \varepsilon_F$ consistent with the LDA calculations.

Figure 13 shows results of a calculation where the O at-

oms have been moved to the apex positions. We find that this leads to a fairly small change of the spectrum. In the non-self-consistent calculation for the La_2CuO_4 structure, the locally screened peak is somewhat more pronounced. This is due to the nonbonding O orbitals around the central Cu atom which interact very weakly with other states and therefore form a narrow locally screened peak. It is apparent that the absence of O apex atoms is not the main reason for the unusual spectrum of Nd_2CuO_4 . Instead we conclude that the strong coupling to high-lying conduction states mentioned above play an important role for this compound. In this vein, Fig. 14 shows that the leading peak of Nd_2CuO_4 occurs at somewhat larger binding energy in Nd_2CuO_4 than in the other compounds. This is in particular due to the strong coupling to high-lying conduction states, which lowers the energy of the initial state. In the final ground state (which means the ground state of the system with the core hole), the hopping to the conduction state lowers the final ground state energy much less than in the initial state. This follows since the energy required for a 3*d* electron to hop into the conduction band is much higher, due to the presence of the core hole attraction U_{dc} . The result is a larger binding energy.

In conclusion, the different shape of the Nd_2CuO_4 spectrum can broadly speaking be explained by its different electronic structure. The shape of the spectra of two-dimensional cuprates in general shows a greater variety than do those of one- and zero-dimensional cuprates, which may indicate a greater variety as regards the features of their electronic structure. Nevertheless, we conclude that the principle mechanism for the screening in the different compounds is the same modified by effects due to the broad antibonding valence band and mixing effects with higher lying states. The role of the apex position is rather to influence the electronic structure as a whole, than to participate directly in the screening of the core hole itself.

VII. SUMMARY

In order to examine the similarities and differences in the screening response of the valence electron system to the creation of a core hole, we have investigated single crystals of the number of cuprate systems containing 2D Cu-O networks with high-resolution core level photoemission. Specifically, the halooxocuprates $\text{Ca}_2\text{CuO}_2\text{Cl}_2$, $\text{Sr}_2\text{CuO}_2\text{Cl}_2$, and $\text{Sr}_2\text{CuO}_2\text{Br}_2$, the *p*-type HTSC compound $\text{Bi}_2\text{Sr}_2\text{CaCu}_2\text{O}_{8+\delta}$ and the undoped parent compound of the electron-doped superconductors Nd_2CuO_4 have been examined. Based upon a systematic analysis of the core level spectra of the substituent elements, we found that the cleavage surfaces of the halooxocuprates were almost free of contamination and stable for several days in UHV. The same holds for $\text{Bi}_2\text{Sr}_2\text{CaCu}_2\text{O}_{8+\delta}$ but not for Nd_2CuO_4 , which showed moderate oxide-related contamination at the surface. The presence of a clear second calcium signal was found in the Ca-2*p* spectrum of $\text{Ca}_2\text{CuO}_2\text{Cl}_2$, which may be due to disorder on the Ca sublattice.

As regards the Cu-2*p*_{3/2} spectra, the shape of the main line for all three halooxocuprates was found to be almost identical. $\text{Bi}_2\text{Sr}_2\text{CaCu}_2\text{O}_{8+\delta}$ showed a similar shape, but the

main line of Nd_2CuO_4 is obviously narrower. In order to gain an insight into the processes underlying both the similarities and differences in the $\text{Cu-}2p_{3/2}$ main line spectra, an Anderson impurity model was fitted to the experimental data. It describes the overall energy spread of the main line quite well and reproduces the Nd_2CuO_4 main line accurately. For the other compounds, structure in the main line observed in experiment seems to be missing in the theoretical curves. Based on the calculations, we assign the high-binding-energy shoulder of the main line to a locally screened channel and the leading peak (at lowest binding energy) to nonlocally screened final states. In the case of Nd_2CuO_4 , we find in

addition that the spectrum is influenced by coupling of the valence states to higher-lying conduction band states. Apart from the observed insensitivity of the experimental $\text{Cu-}2p_{3/2}$ main lines to the identity of the apex atom in the halooxocuprates (Cl or Br), a theoretical treatment of the Nd_2CuO_4 $\text{Cu-}2p_{3/2}$ main line showed that the impact of the apex position on the core hole screening is rather weak.

ACKNOWLEDGMENTS

We are grateful to the DFG (FI 439/10-1) for financial support of this work.

- ¹J. G. Bednorz and K. A. Müller, *Z. Phys. B: Condens. Matter* **64**, 189 (1986).
- ²Z. X. Shen, J. W. Allen, J. J. Yeh, J. S. Kang, W. Ellis, W. Spicer, I. Lindau, M. B. Maple, Y. D. Dalichaouch, M. S. Torikachvili, J. Z. Sun, and T. H. Geballe, *Phys. Rev. B* **36**, 8414 (1987).
- ³A. Fujimori, S. Takekawa, E. Takayama-Muromachi, Y. Uchida, A. Ona, T. Takahashi, Y. Okabe, and H. Katayama-Yoshida, *Phys. Rev. B* **39**, 2255 (1989).
- ⁴C. N. R. Rao, G. Ranga Rao, M. K. Rajumon, and D. D. Sarma, *Phys. Rev. B* **42**, 1026 (1999).
- ⁵G. van der Laan, C. Westra, C. Haas, and G. A. Sawatzky, *Phys. Rev. B* **23**, 4369 (1981).
- ⁶J. M. Tranquada, S. M. Heald, W. Kunnmann, A. R. Moodenbough, S. L. Qiu, X. Youwen, and P. K. Davies, *Phys. Rev. B* **44**, 5176 (1991).
- ⁷K. Karlsson, O. Gunnarsson, and O. Jepsen, *J. Phys.: Condens. Matter* **4**, 2801 (1992).
- ⁸M. A. van Veenendaal and G. A. Sawatzky, *Phys. Rev. Lett.* **70**, 2459 (1993); M. A. van Veenendaal, H. Eskes, and G. A. Sawatzky, *Phys. Rev. B* **47**, 11 462 (1993).
- ⁹M. A. van Veenendaal, G. A. Sawatzky, and W. A. Groen, *Phys. Rev. B* **49**, 1407 (1994).
- ¹⁰K. Karlsson, O. Gunnarsson, and O. Jepsen, *Phys. Rev. Lett.* **82**, 3528 (1999).
- ¹¹F. Parmigiani, L. Depero, T. Minerva, and J. B. Torrance, *J. Electron Spectrosc. Relat. Phenom.* **58**, 315 (1992).
- ¹²T. Böske, O. Knauff, R. Neudert, M. Kielwein, M. Knupfer, M. S. Golden, J. Fink, H. Eisaki, S. Uchida, K. Okada, and A. Kotani, *Phys. Rev. B* **56**, 3438 (1997).
- ¹³T. Böske, K. Maiti, O. Knauff, K. Ruck, M. S. Golden, G. Krabbes, J. Fink, T. Osafune, N. Motoyama, H. Eisaki, and S. Uchida, *Phys. Rev. B* **57**, 138 (1998).
- ¹⁴C. L. Teske and Hk. Mueller-Buschbaum, *Z. Anorg. Allg. Chem.* **371**, 325 (1969).
- ¹⁵Y. Mizuno, T. Tohyama, S. Maekawa, T. Osafune, N. Motoyama, H. Eisaki, and S. Uchida, *Phys. Rev. B* **57**, 5326 (1998).
- ¹⁶K. Okada and A. Kotani, *J. Electron Spectrosc. Relat. Phenom.* **86**, 119 (1997).
- ¹⁷C. Waidacher, J. Richter, and K. W. Becker, *Europhys. Lett.* **47**, 77 (1999).
- ¹⁸PHI 5600 of Perkin Elmer corporation, Eden Prairie, Minnesota 55344.
- ¹⁹L. L. Miller, X. L. Wang, S. X. Wang, C. Stassis, D. C. Johnston, J. Faber, Jr., and C. K. Loong, *Phys. Rev. B* **41**, 1921 (1990).
- ²⁰H. Takagi, S. Uchida, and Y. Tokura, *Phys. Rev. Lett.* **62**, 1197 (1989).
- ²¹G. Yang, J. S. Abell, and C. E. Gough, *Appl. Phys. Lett.* **75**, 1955 (1999).
- ²²O. Gunnarsson and K. Schönhammer, in *Handbook of the Physics and Chemistry of Rare Earths*, edited by K. A. Gschneider, Jr., L. R. Eyring, and S. Huefner (North-Holland, Amsterdam, 1987), Vol. 10, p. 103.
- ²³O. K. Andersen, *Phys. Rev. B* **12**, 3060 (1975).
- ²⁴O. Gunnarsson, O. K. Andersen, O. Jepsen, and J. Zaanen, *Phys. Rev. B* **39**, 1708 (1989).
- ²⁵O. Gunnarsson and K. Schönhammer, *Phys. Rev. Lett.* **50**, 604 (1983).
- ²⁶L. L. Miller (private communication).
- ²⁷C. Hinnen, C. Nguyen van Huong, and P. Marcus, *J. Electron Spectrosc. Relat. Phenom.* **73**, 293 (1994).
- ²⁸Z. Hiroi, N. Kobayashi, and M. Takano, *Nature (London)* **371**, 139 (1994).
- ²⁹S. Adachi, T. Tatsuki, T. Tamura, and K. Tanabe, *Chem. Mater.* **10**, 2860 (1998).
- ³⁰Instruction manual, Perkin Elmer Corporation, 1993.
- ³¹F. Ronning, C. Kim, D. L. Feng, D. S. Marshall, A. G. Loeser, L. L. Miller, J. N. Eckstein, I. Bozovich, and Z.-X. Shen, *Science* **282**, 2067 (1998).
- ³²M. Qvarford, S. Söderholm, G. Chiaia, R. Nyholm, J. N. Andersen, I. Lindau, U. O. Karlsson, L. Leonyuk, A. Nilsson, and N. Martensson, *Phys. Rev. B* **53**, 14 753 (1996).
- ³³H. Yamamoto, M. Naito, and H. Sato, *Phys. Rev. B* **56**, 2852 (1997).
- ³⁴T. R. Cummins and R. G. Egdell, *Phys. Rev. B* **48**, 6556 (1993).
- ³⁵G. Chiaia, M. Qvarford, I. Lindau, S. Söderholm, U. O. Karlsson, S. A. Flodström, L. Leonyuk, A. Nilsson, and N. Martensson, *Phys. Rev. B* **51**, 1213 (1995).
- ³⁶Y. Tokura, S. Kohihara, T. Arima, H. Takagi, S. Ishibashi, T. Ido, and S. Uchida, *Phys. Rev. B* **41**, 11 657 (1990).
- ³⁷O. K. Andersen and O. Jepsen, *Phys. Rev. Lett.* **53**, 2571 (1984).
- ³⁸A. Fujimori, Y. Tokura, H. Eisaki, H. Takagi, and S. Uchida, *Phys. Rev. B* **42**, 325 (1990).
- ³⁹K. Karlsson, O. Gunnarsson, and O. Jepsen, *Int. J. Mod. Phys. B* **14**, 3791 (2000).
- ⁴⁰B. Grande and Hk. Müller-Buschbaum, *Z. Anorg. Allg. Chem.* **417**, 68 (1975).

- ⁴¹B. Grande and Hk. Müller-Buschbaum, *Z. Anorg. Allg. Chem.* **429**, 88 (1977).
- ⁴²B. Grande and Hk. Müller-Buschbaum, *Z. Anorg. Allg. Chem.* **433**, 152 (1977).
- ⁴³Hk. Müller-Buschbaum and W. Wollschläger, *Z. Anorg. Allg. Chem.* **414**, 76 (1975).
- ⁴⁴J. M. Tarascon, W. R. McKinnon, P. Barboux, D. M. Hwang, B. G. Bagley, L. H. Greene, G. W. Hull, Y. LePage, N. Stoffel, and M. Giroud, *Phys. Rev. B* **38**, 8885 (1988).
- ⁴⁵R. P. Vasquez, *J. Electron Spectrosc. Relat. Phenom.* **66**, 241 (1994); R. P. Vasquez, D. L. Novikov, A. J. Freeman, and M. P. Siegal, *Phys. Rev. B* **55**, 14 623 (1997); R. P. Vasquez, M. P. Siegal, D. L. Overmyer, Z. F. Ren, J. Y. Lao, and J. H. Wang, *ibid.* **60**, 4309 (1999).